OBSERVATIONS OF H II REGIONS AT 1400 MC

C. R. Lynds

Abstract

Several H II regions have been mapped at a frequency of 1400 Mc. Flux densities have been determined for the observed sources and compared with previously published results.

During the early part of 1960 a survey of a number of extended H II regions was made at a frequency of 1400 Mc with the 85-foot Tatel telescope of the National Radio Astronomy Observatory. The receiver used was a Ewen-Dae hydrogen line radiometer working without image rejection at a local oscillator frequency of 1400 Mc and a 6 Mc bandwidth. The antenna pattern exhibits nearly perfect axial symmetry and has a width at half-power of approximately $0°59$. Because of the strongly tapered illumination of the primary surface by the feed, sidelobe effects are entirely negligible for all sources except the sun.

The observational program was designed to yield radio-frequency brightness distributions over regions of approximately 6° x 6° surrounding the following objects: NGC 7822, IC 1795, NGC 1499, IC 410, NGC 7000, IC 1396, and Cas A. The observations were taken in the form of scans in declination with the receiver output being presented in analog form on a Sanborn strip-chart recorder and in digital form on printed tape and on punched teletype tape. All observations on punched tape were averaged and reduced automatically on an IBM 610 computer. The declination scans were obtained by scanning alternately north and south to eliminate the linear component of secular receiver drift. At least two pairs of scans were taken at each right ascension setting; more were taken for regions of special interest and where the first observations were suspect. The scan speed was approximately $1°5$ per minute and the integration time for each digitized observation was 10 seconds. In most cases the scans at various right ascensions were related to a common base by means of drifts in right ascension. An occasional check of receiver sensitivity was afforded by observations of the output of a standard noise tube of demonstrated stability. An equivalent antenna temperature of 36 °K for the injected calibration signal has been measured by H. Hvatum by means of comparisons with a thermal load. The calibration of the system sensitivity was obtained by observing the source 16N0A for which Heeschen (1961) has determined an accurate source-to-Cas A ratio of 0.0178 ± 0.0004. The flux density of Cas A at 1400 Mc as determined at this observatory (Hvatum, 1960) is 2.5×10^{-23} w m^{-2} (c/s)$^{-1}$. The resulting flux 44.5×10^{-26} w m^{-2} (c/s)$^{-1}$ was adopted for 16N0A. The flux density of a source is given by

$$S = \frac{2k}{\lambda^2} \frac{1}{(1-L) E_b} \int_S \Delta T_a(\theta, \phi) \, d\Omega, \tag{1}$$

where L represents any ohmic losses suffered by the signal before the point of injection of the calibration signal. The integral is taken over the source. ΔT_a is the antenna temperature and E_b is the beam efficiency defined by

$$E_b = \frac{\int_b f(\theta, \phi) \, d\Omega}{\int_{4\pi} f(\theta, \phi) \, d\Omega} \qquad (2)$$

where $f(\theta, \phi)$ gives the directional response of the antenna and the upper integral is to be taken over the main beam of the antenna. The observations of 16N0A give 6.168×10^{-4} steradian for the integral of ΔT_a. The resulting value for $(1 - L) E_b$ is 0.83. This is perhaps a little higher than we would reasonably expect. The value for the integral of ΔT_a, together with the observed maximum antenna temperature of 5.2 °K for 16N0A, indicates an effective solid angle for the main beam of 1.18×10^{-4} steradian. The brightness temperature T_b is related to the antenna temperature by

$$k \, \Delta T_a = \frac{1}{2} (1 - L) \, \lambda^2 \, E_b \, \frac{\int_b f(\theta, \varphi) \frac{2k}{\lambda^2} T_b(\theta, \varphi) \, d\Omega}{\int_b f(\theta, \varphi) \, d\Omega} \ , \qquad (3)$$

which reduces to

$$\Delta T_a = (1 - L) \, E_b \, T_{be}, \qquad (4)$$

where T_{be} is the effective brightness temperature and is the average of T_b over the main beam with $f(\theta, \varphi)$ as the weighting function. For the present observations the effective brightness temperature may be computed from

$$T_{be} = 1.20 \, \Delta T_a. \qquad (5)$$

The results of the observations are presented as radio brightness distributions in Figures 1 through 7. No attempt has been made to correct the distributions for the effects of broadening by the antenna beam. The contour intensities are given in the legend for each figure in units corresponding to 1.33 °K antenna temperature and 1.59 °K effective brightness temperature. Portions of the radio brightness distributions have been reproduced without coordinate grid and superimposed on the corresponding optical fields taken from the "E" emulsion prints of the National Geographic Society 48-inch Schmidt survey. These are shown in Figures 8 through 14. The contours have been drawn on coordinate projections produced especially for the 48-inch survey and the accuracy of the registration is of the order of one or two minutes of arc, somewhat more for the composite prints. A brief description of each of the regions follows.

NGC 7822. —— The contours in this region (Figures 1 and 8) show an extended source of maximum intensity 5.2 units, corresponding well in position and brightness distribution with the emission nebulosity in the region. The most intense part of the source seems to lie in a heavily obscured region near the center of the optical object. The radio source 00N6A associated with the remnants of the supernova of 1572 appears just at the southern edge of the region surveyed.

IC 1795. —— The brightness distribution in this region (Figures 2 and 9) corresponds very well with that found by Westerhout (1958) at 1390 Mc. The most intense part of the extended source seems to be associated with the strong emission nebula IC 1795. The

maximum intensity is about 9.0 units. The lower intensity contours extend south-east in the direction of the emission nebula IC 1805 and the original records show a clear resolution of a source corresponding in position with the brightest parts of this nebula. Radio emission from another H II region, IC 1848, is indicated at the east edge of the field. In addition the discrete source 3C 69 can be seen on the original records but its intensity lies just below that of the lowest contour in Figure 2.

NGC 1499. —— The brightness distribution of this region (Figures 3 and 10) shows a fairly weak extended source of maximum intensity 1.6 units corresponding very well in position and shape with the emission nebula NGC 1499, the California Nebula. The author is not aware of any previous radio observations of this object. The discrete source 3C 111 appears on the eastern edge of the survey region.

IC 410. —— The contours in Figures 4 and 11 indicate a source corresponding with IC 410 having a maximum intensity of 1.9 units. The lowest contour shows an extension in the direction of the H II region IC 405. The extension is very weak and does not show especially good position correspondence with the brightest parts of the nebula but is nevertheless probably associated with it.

NGC 7000. —— Figures 5 and 12 show the radio brightness distribution in the region of the North American Nebula. This region is near the Cygnus X complex and, as in that case, there is evidence for strong foreground obscuration. There is a very poor correspondence between the strongest sources and the regions of strongest Hα emission. The strong source at $\alpha = 20^h 38^m5$, $\delta = +41° 50'$ coincides with only a very faint nebulosity and possibly we cannot see optically the true source of the radio emission. Another strong source lies directly in the dark bay between the optically bright NGC 7000 and the fainter "Pelican" nebula. Part of the outline of NGC 7000 and some other features are represented fairly well by the lower contours of radio brightness.

IC 1396. —— The radio observations of this object (Figures 6 and 13) indicate a rather weak extended source having a brightness distribution somewhat similar to that of the optical emission. The maximum intensity of the source is only 1.5 units. The brightness distribution becomes complicated toward the southern edge of the region. The optical object is distinguished by the presence of "elephant trunks".

Cas A. —— The region of Cas A was studied in considerably greater detail than the other fields so that the effect of additional sources in the vicinity of Cas A could be removed from the response of the Cas A calibration horn operated at this observatory. The present observations, illustrated in Figures 7 and 14, indicate three sources associated with H II regions and possibly a fourth near $\alpha = 23^h 00^m$, $\delta = +58° 36'$. It appears that the H II regions have not been detected previously, possibly because of their proximity to the very strong source Cas A.

The sources observed in the survey regions are listed in Table 1. Also included in the table is one weak source found to be apparently associated with the σ Sco nebulosity. This is the only source found in a 6° x 6° region centered on α Sco. The table gives, for each source, in successive columns the name, the right ascension and declination for 1950, the galactic coordinates on the new IAU system, the maximum antenna temperature observed, the flux density determined from the present observations, the flux density at 1390 Mc given by Westerhout (1958), the flux density at 960 Mc given by Wilson and Bolton (1960) or Harris and Roberts (1960), and, in the last column, other designations for the source. The references associated with the catalogue designations given in Table 1 and the Notes are

TABLE 1

RADIO SOURCES OBSERVED AT 1400 MC

No.	Name	α	δ	l*	b*	T_a Max.	S 1400	S 1390	S 960	Other Designations
1	NGC 7822	00h 01m +66° 55'	118°	+5°	6.9	185	160	220	CTB 2, W 1
2	NGC 7822	Central Component			6.9	130	40		
3	SN 1572	00 22.5 +64 20:	120	+2	3.8	37		57	CTB 4
4	IC 1795	02 22 +61 50	134	+1	11.9	152	170	400	CTB 9, W 3
5	IC 1805	02 30: +61 05:	135	+1	4.4	122	90		CTB 9, W 4
6	3C 69	02 34 +59 10	136	-1	0.4	3:		25	CTB 10
7	IC 1848						120	175	CTB 11, W 5
8	NGC 1499	03 58: +36 15:	160	-12	2.1	76			
9	3C 111	04 15: +37 57	162	-9	1.5	14:		20	CTA 30
10	IC 405	05 13: +34 10:	172	-2	0.9	29		40	CTB 16
11	IC 410	05 19.3 +33 23	174	-2	2.5	46	77	60	CTB 17, W 8
12	σ Sco	16 17 -25 35	351	+17	0.7	21			
13		20 34: +46 45	85	+4	3.3	50:	85	100	CTB 95, W 71
14		20 35.5 +45 15	84	+3	0.4	3			
15		20 38.5 +41 50	82	0	15.9	290	270		W 75
16		20 48.9 +42 07	83	-1	2.7	24			
17		20 53.2 +43 45	85	-1	5.7	377	550	350	CTB 100, W 80
18	IC 1396	21 38 +57 30:	100	+4	2.0	116		210	CTB 105
19		21 53: +57 25	101	+3	0.8	7			
20		23 00 +58 36	109	-1	1.9	20:		75	CTB 109
21	NGC 7538	23 12.4 +61 12	112	+1	2.0	19			
22	S 157	23 12.7 +59 38	111	-1	2.1	22			
23	NGC 7635	23 18.8 +60 46	112	0	1.5	14:			
24	Cas A	23 21.1 +58 28	112	-1		2500*	3100	3120	CTB 110, W 81
25		23 35 +58 40	114	-3	0.9	8			

: Poorly defined or uncertain value.
* Adopted value.

NOTES TO TABLE 1

1, 2. —— Like the optical object, the radio source seems to consist of a strong central source with partially resolved outlying sources. The flux density given for source No. 2 is based on this interpretation. Observations at 9.6 cm by A. D. Kuzmin, et al. (1960) indicate a flux density of 160 x 10^{-26} w m^{-2} $(c/s)^{-1}$.

3. —— Other designations for this source are CTA 2, 3C 10, and HB 1. The 159 Mc fluxes quoted in the literature are 110 x 10^{-26} w m^{-2} $(c/s)^{-1}$ (3C catalogue) and 170 x 10^{-26} w m^{-2} $(c/s)^{-1}$(Brown and Hazard,1953). The flux density at 9.6 cm is 30 x 10^{-26} w m^{-2} $(c/s)^{-1}$ (Kuzmin, et al. 1960).

4, 5. —— The 960 Mc flux refers to the combination of the two sources.

6. —— The flux density at 159 Mc given in the 3C catalogue is 23 x 10^{-26} w m^{-2} $(c/s)^{-1}$. It seems that at least one of the flux values is in error.

7. —— Only the western edge of this extended source was observed in the survey.

9. —— This source is on the edge of the survey region and the flux given is only an estimate. The flux density at 159 Mc given in the 3C catalogue is 60 x 10^{-26} w m^{-2} $(c/s)^{-1}$.

11. —— This H II region has been observed at 9.6 cm by Kuzmin, et al. (1960) who obtained a flux density of 70 x 10^{-26} w m^{-2} $(c/s)^{-1}$.

12. —— A faint emission nebula near σ Sco.

13. —— May be associated with S 115.

15. —— A faint H II region appears on the Palomar 48-inch plate.

16. —— May be associated with IC 5068.

17. —— The most intense part of this extended source lies between NGC 7000 and IC 5067.

18. —— S 131.

20. —— May be associated with two small H II regions S 152 and S 153.

CTA..... Harris and Roberts (1960),
CTB..... Wilson and Bolton (1960),
W....... Westerhout (1958),
3C ...... Edge, et al. (1959),
HB...... Brown and Hazard (1953), and
S........ Sharpless (1959).

The flux densities are given in units of 10^{-26} w m^{-2} (c/s)$^{-1}$. The fluxes for the present observations were determined by planimetering the averaged scans.

The data given in Table 1 demonstrate clearly the difficulty in determining accurate spectral indices for extended sources from observations at different frequencies obtained with instruments of different angular resolution. A comparison of the present data with the fluxes derived by Westerhout at nearly the same frequency and angular resolution shows that the average flux for the objects in common is about the same but that there is a rather large divergence in the fluxes for individual sources. The differences most likely arise from differing criteria defining the angular extent of extended sources, differing interpretations of the brightness distributions for overlapping sources, and the rather large effects caused by a different assessment of the distributive nature of the galactic background. In addition a published flux has often been determined from the maximum observed brightness temperature and either optical or radio estimates of the angular extent of the source. In the absence of detailed knowledge of the brightness distribution this procedure can lead to erroneous results.

The interpretive difficulties mentioned above show up quite clearly in the case of NGC 7822. Here the flux density of the entire source given by Westerhout and that derived from the present data agree fairly well while the determination of that part of the radiation due to a "central component" has lead to quite a different result in the two cases. Such difficulties are enhanced when the attempt is made to compare results obtained with different angular resolutions as is the usual case for observations at different frequencies. A partial solution to these problems can be effected by smoothing the higher resolution observations to correspond with the low resolution observations and by treating both bodies of data in a well defined manner. Likewise, low resolution data can often be corrected for the effects of antenna smoothing by making use of the information available in the data of higher angular resolution. In both cases it should be possible to make fairly good estimates of the spectral characteristics of extended sources.

A comparison of the average of the 1390 Mc and 1400 Mc fluxes and the fluxes at 960 Mc for the H II regions indicates an average spectral index of about -0.6. However, for the reasons mentioned above, this result should not be taken as reliable. Let us consider a few of the sources individually.

NGC 7822. —— The average 22 cm flux and the 9.6 cm flux indicate a reasonably flat spectrum. The 960 Mc flux would seem to be too large, possibly because of an overestimate of the angular size of the radio source.

IC 1795 plus IC 1805. —— The 960 Mc flux and the 22 cm flux indicate a spectral index of about -1.1, an unexpectedly large value. In view of the agreement between the 1390 Mc and 1400 Mc results, it is likely that the 960 Mc flux is an overestimate. The same situation seems to exist for the source associated with IC 1848.

IC 410. —— The fluxes at 960 Mc and 9.6 cm together with the average flux at 22 cm indicate a fairly reasonable value of +0.2 for the spectral index. The large difference between the 1390 Mc and 1400 Mc results is difficult to understand.

W 80. —— The discordant results for this source are not surprising in view of the great complexity of the region. However, the indicated weakening of the source at low frequencies may be a result of the region becoming optically thick at 960 Mc.

IC 1396. —— The very steep spectrum indicated for this source is probably erroneous and a result of the complex brightness distribution of the source and the galactic background to the south.

Although the presence of a small non-thermal component to the radiation from Hα emission regions is not to be unexpected, the apparent tendency for relatively large negative spectral indices is probably an observational effect. It seems apparent that an improvement in our knowledge of the physics of emission regions will be made by concerted observational efforts on a few objects rather than by a cursory examination of many objects. It is suggested that it might be worthwhile in the future to observe extended sources with telescope-frequency combinations yielding the same angular resolution.

REFERENCES

Brown, R. Hanbury and Hazard, C. 1953, M. N. , 113, 123.

Edge, D. O. , Shakeshaft, J. R. , McAdam, W. B. , Baldwin, J. E. , and Archer, S. 1959, Mem. R. A. S. , 68, 37.

Harris, D. E. and Roberts, J. A. 1960, Pub. A. S. P. , 72, 273.

Heeschen, D. S. 1961, Ap. J. 133, 332.

Hvatum, H. 1960, private communication.

Kuzmin, A. D. , Levchenko, M. T. , Noskova, R. I. , and Salomonovich, A. E. 1960, Soviet Astr. J. , 37, 975.

Sharpless, Stewart 1959, Ap. J. Supplement, 4, 257.

Westerhout, Gart 1958, B. A. N. , 14, 215.

Wilson, R. W. and Bolton, J. G. 1960, Pub. A. S. P. , 72, 331.
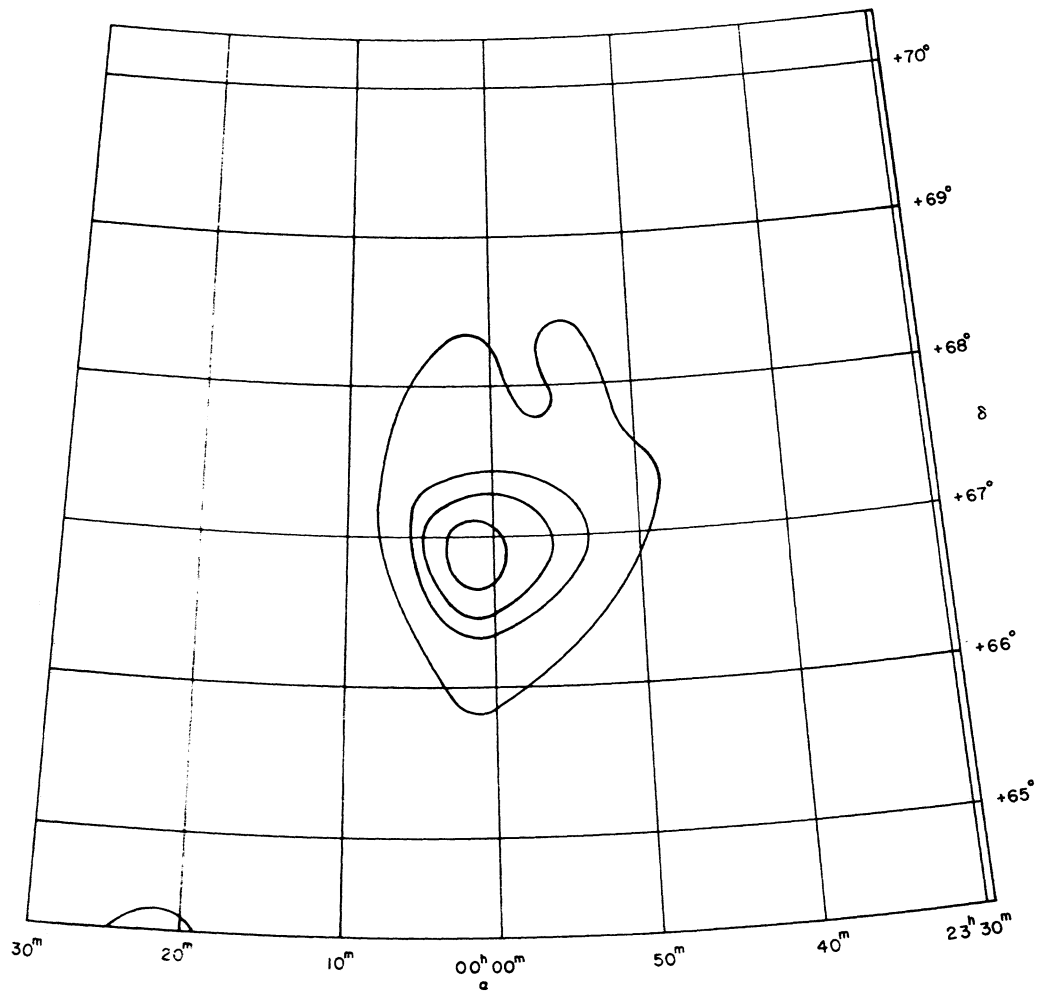
Fig. 1. —— The brightness distribution at 1400 Mc in the region surrounding NGC 7822. The intensities represented by the contours are 1, 2, 3, and 4 units.
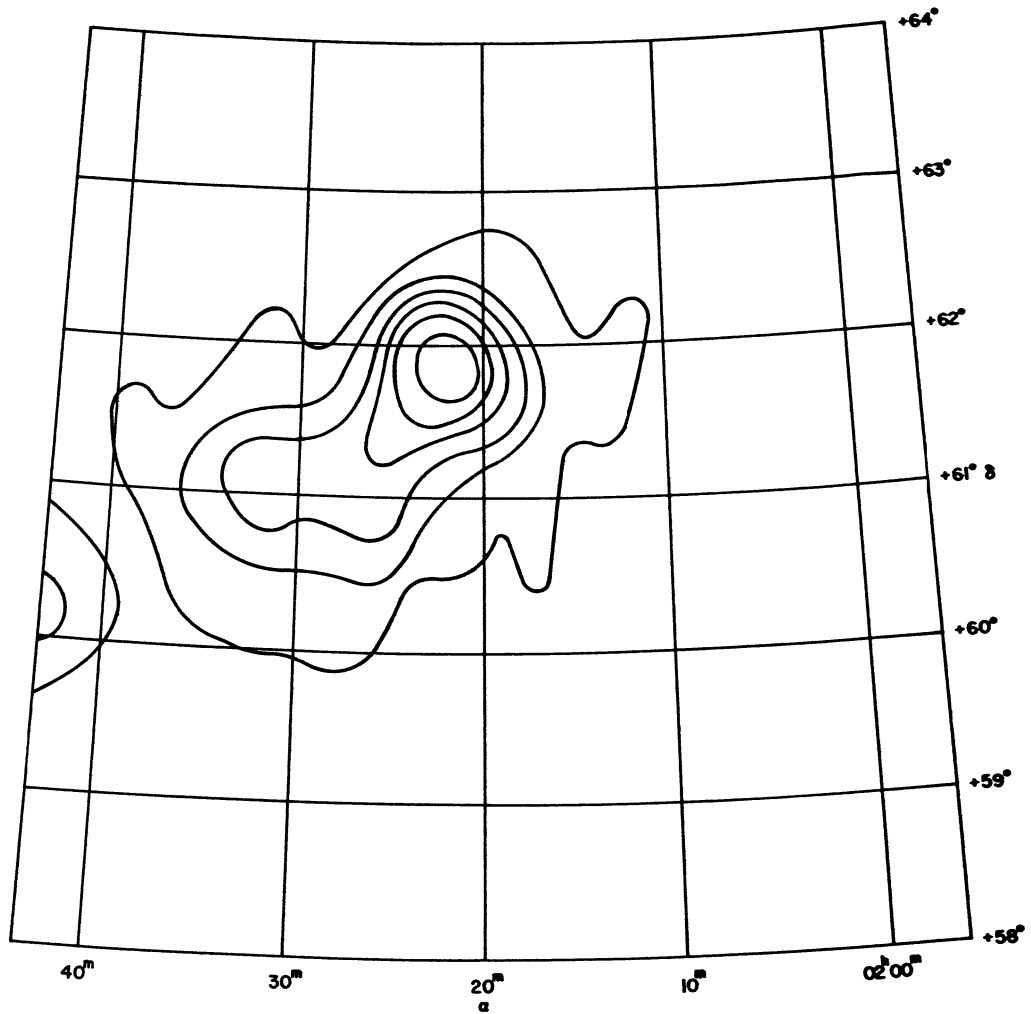
Fig. 2. —— The brightness distribution at 1400 Mc in the vicinity of IC 1795 and IC 1805.
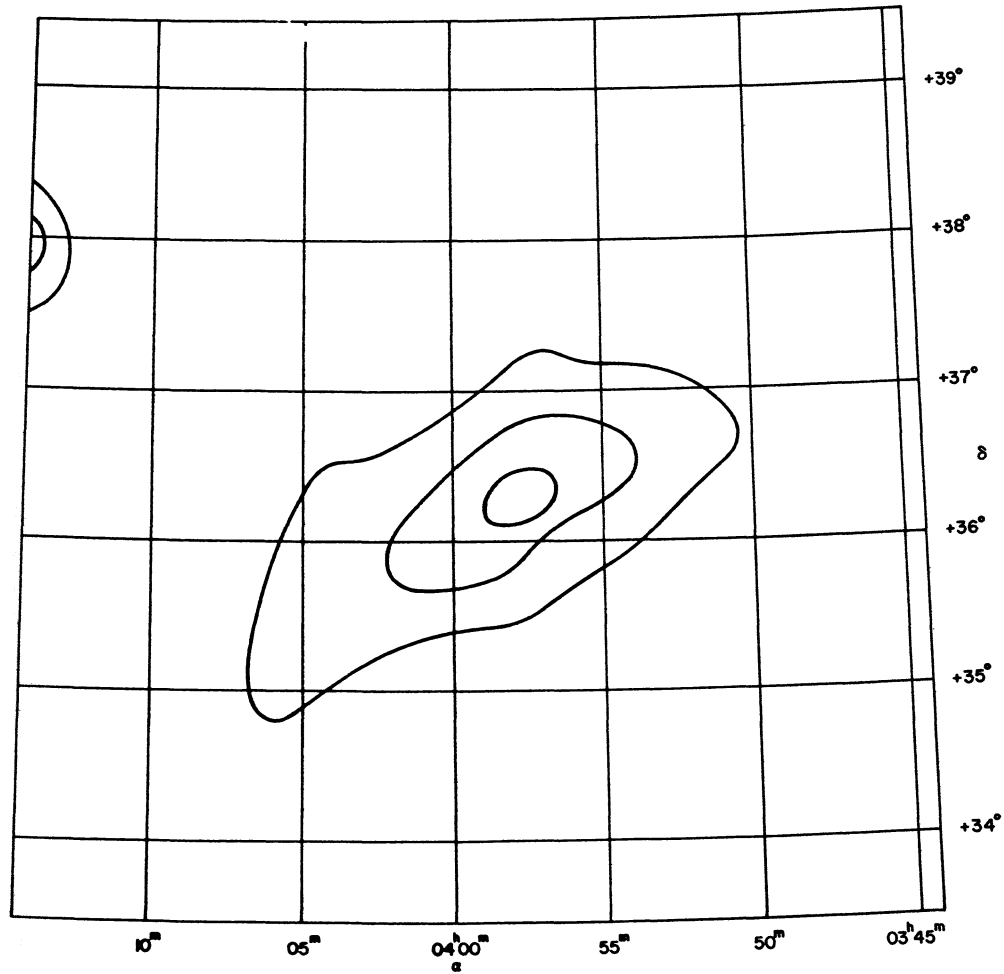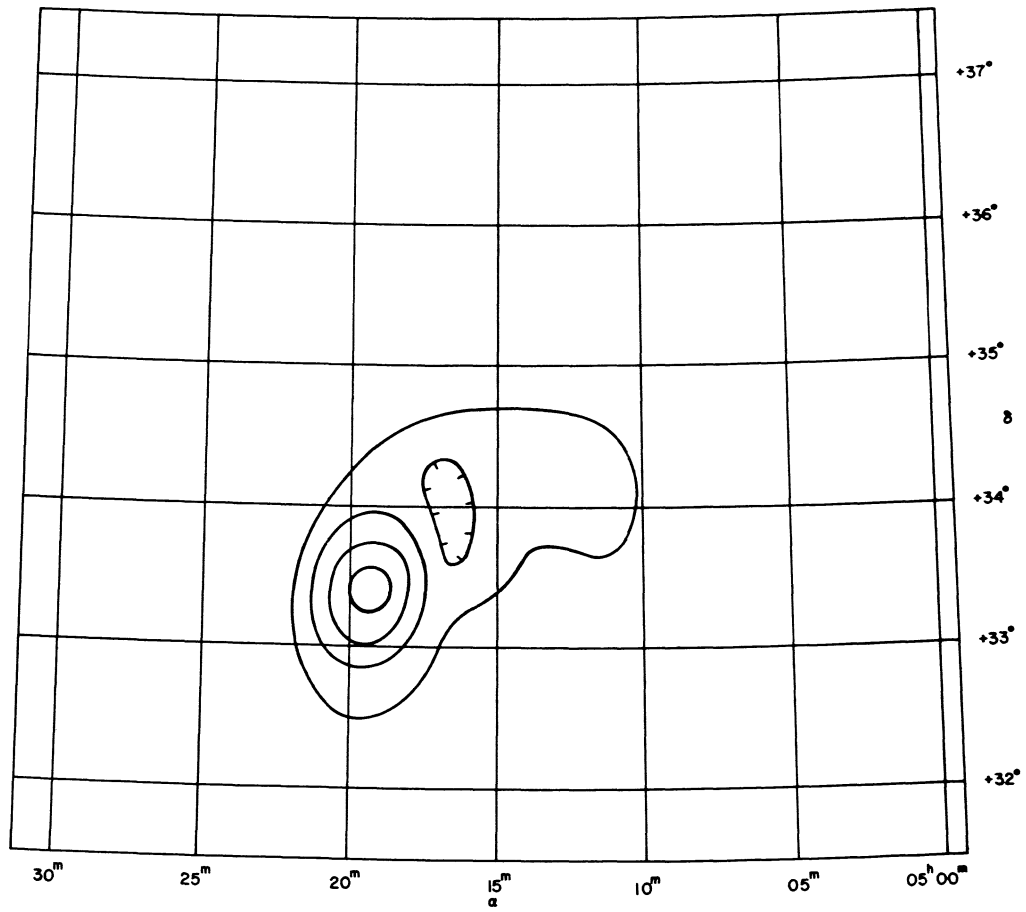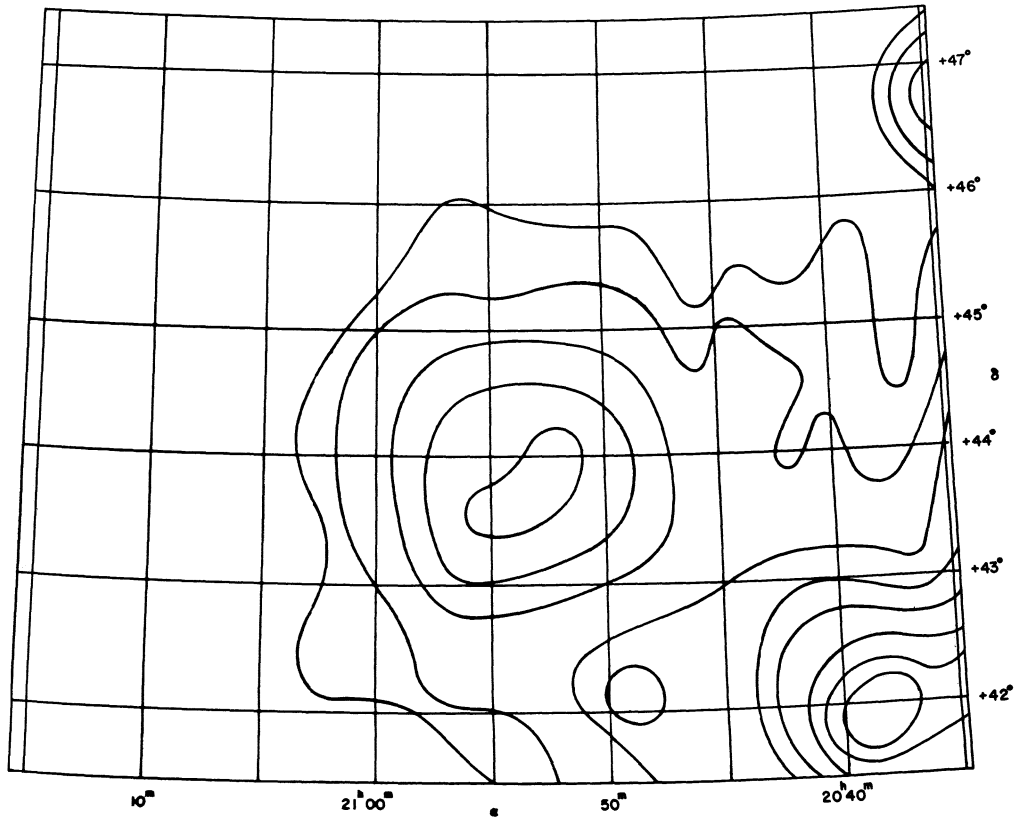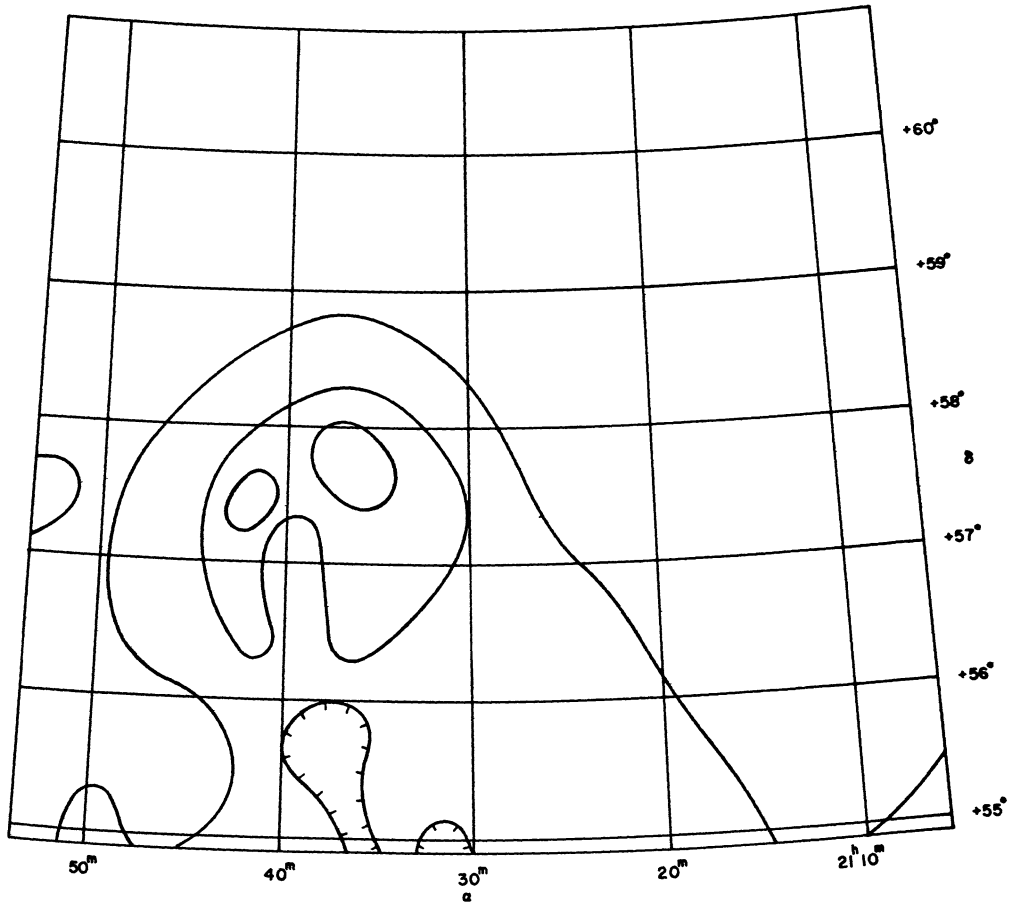The intensities represented by the contours are 1, 2, 3, 4, 5, and 8 units.

Fig. 3. — The brightness distribution at 1400 Mc of NGC 1499, the California Nebula. The intensities represented by the contours are 0.5, 1.0, 1.5 units. The discrete source 3C 111 appears on the eastern edge of the survey region.

Fig. 4. —— The brightness distribution at 1400 Mc in the vicinity of IC 405 and IC 410. The intensities represented by the contours are 0.5, 1.0, 1.5, and 2.0 units.

Fig. 5. — The brightness distribution at 1400 Mc in a region including NGC 7000 and many other complex H II regions. The intensities represented by the contours are 0.5, 1, 2, 3, 4, 6, 8, and 10 units.

Fig. 6. —— The brightness distribution at 1400 Mc in the region of IC 1396. The intensities represented by the contours are 0.5, 1.0, and 1.4 units.
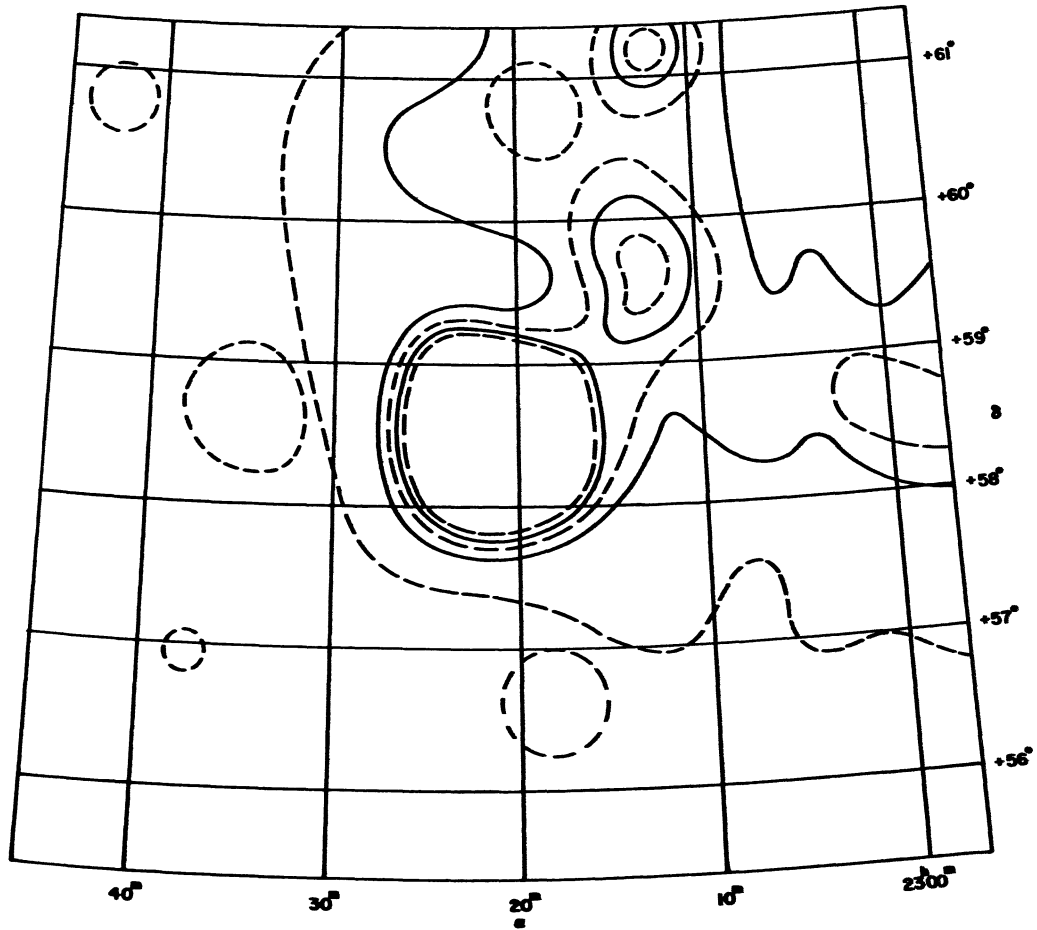
Fig. 7. — The brightness distribution at 1400 Mc in a region centered on the intense non-thermal radio source Cas A. The intensities represented by the contours are 0.5, 1.0, 1.5, 2.0, and 2.5 units. The higher intensity contours for Cas A were not determined.
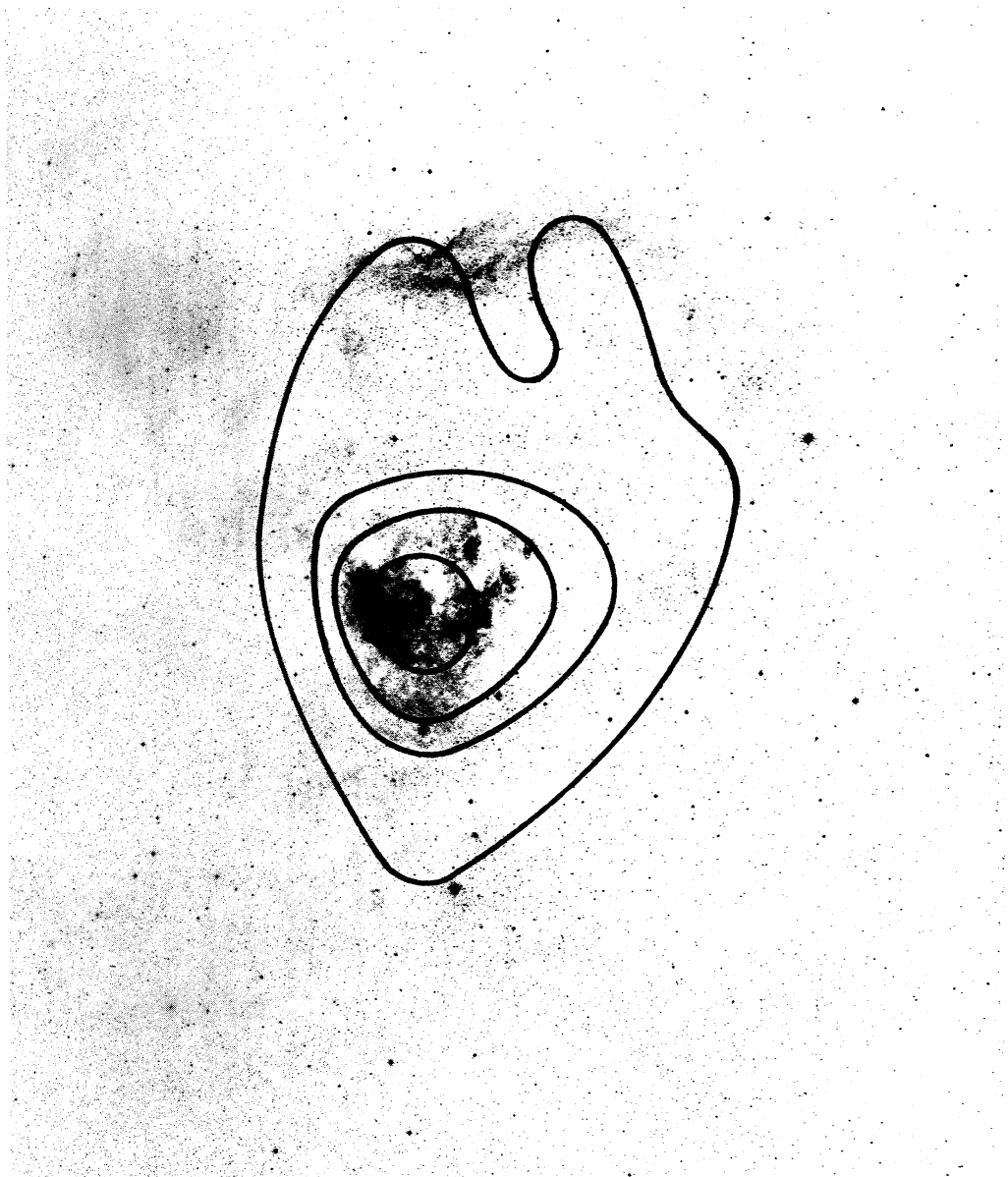
Fig. 8. —— The region of NGC 7822. The radio brightness contours of Figure 1 are shown here superimposed on the corresponding optical field reproduced from an "E" emulsion prints of the National Geographic Society Sky Atlas.
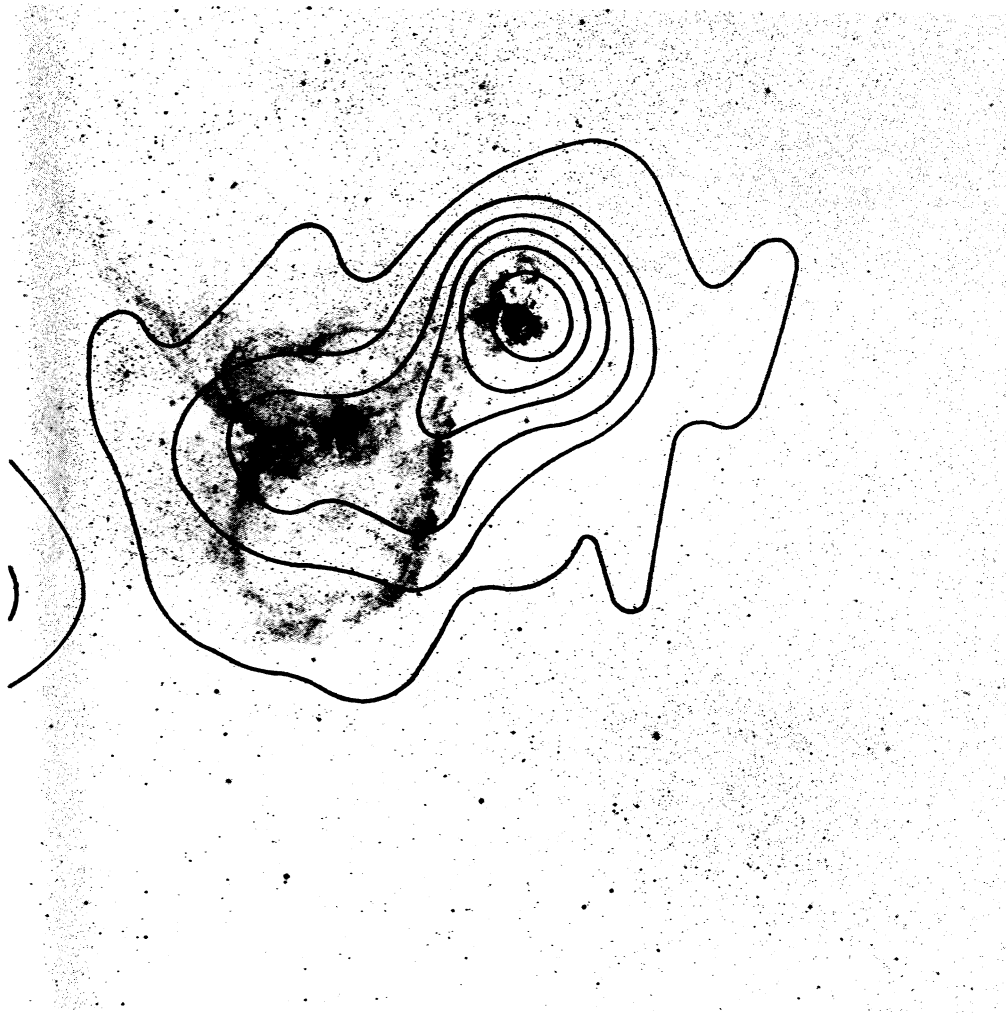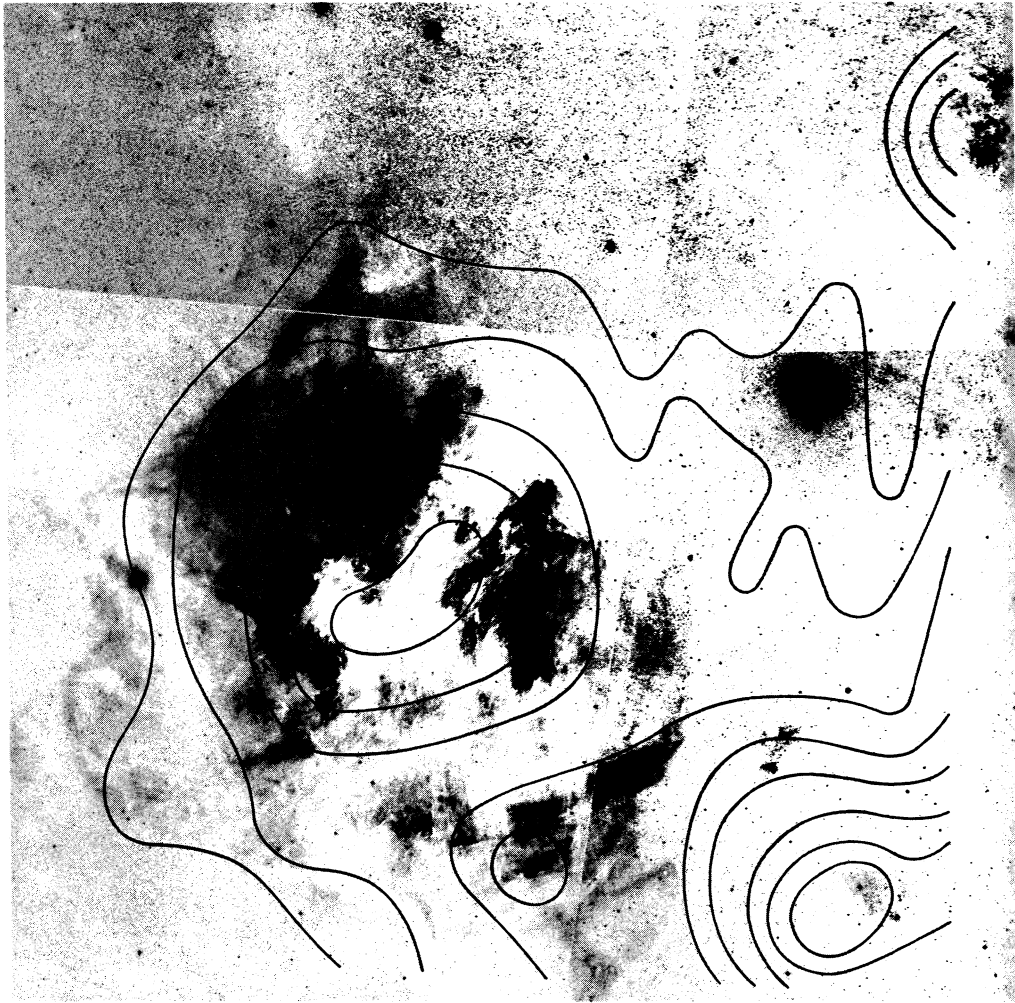
56

Fig. 9. —— The region of IC 1795. The radio brightness contours of Figure 2 are shown here superimposed on the corresponding optical field reproduced from an "E" emulsion print of the National Geographic Society Sky Atlas.
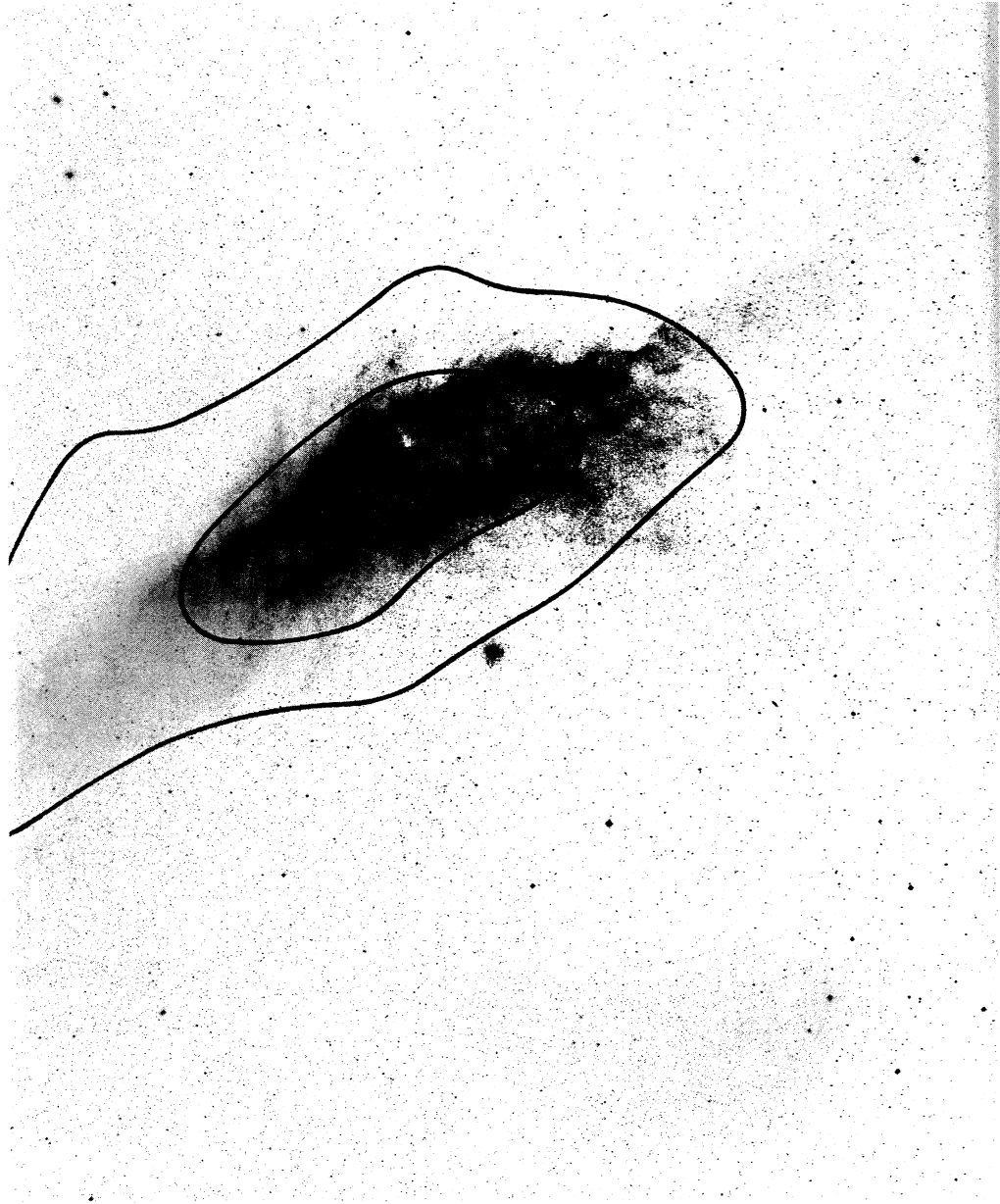
Fig. 10. — The region of NGC 1499. The radio brightness contours of Figure 3 are shown here superimposed on the corresponding optical field reproduced from an "E" emulsion print of the National Geographic Society Sky Atlas.

58
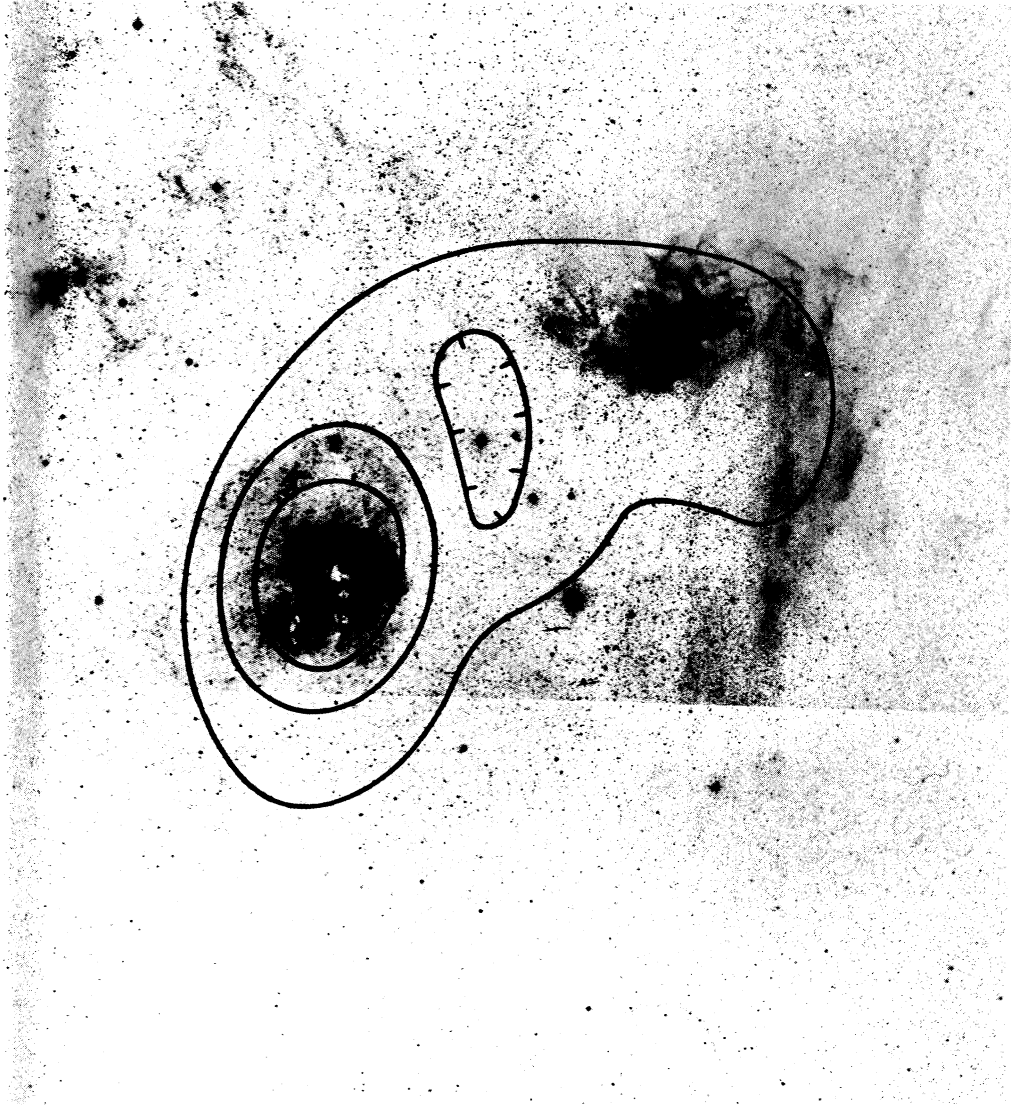
Fig. 11. —— The region of IC 410. The radio brightness contours of Figure 1 are shown here superimposed on the corresponding optical field reproduced from "E" emulsion print of the National Geographic Society Sky Atlas.
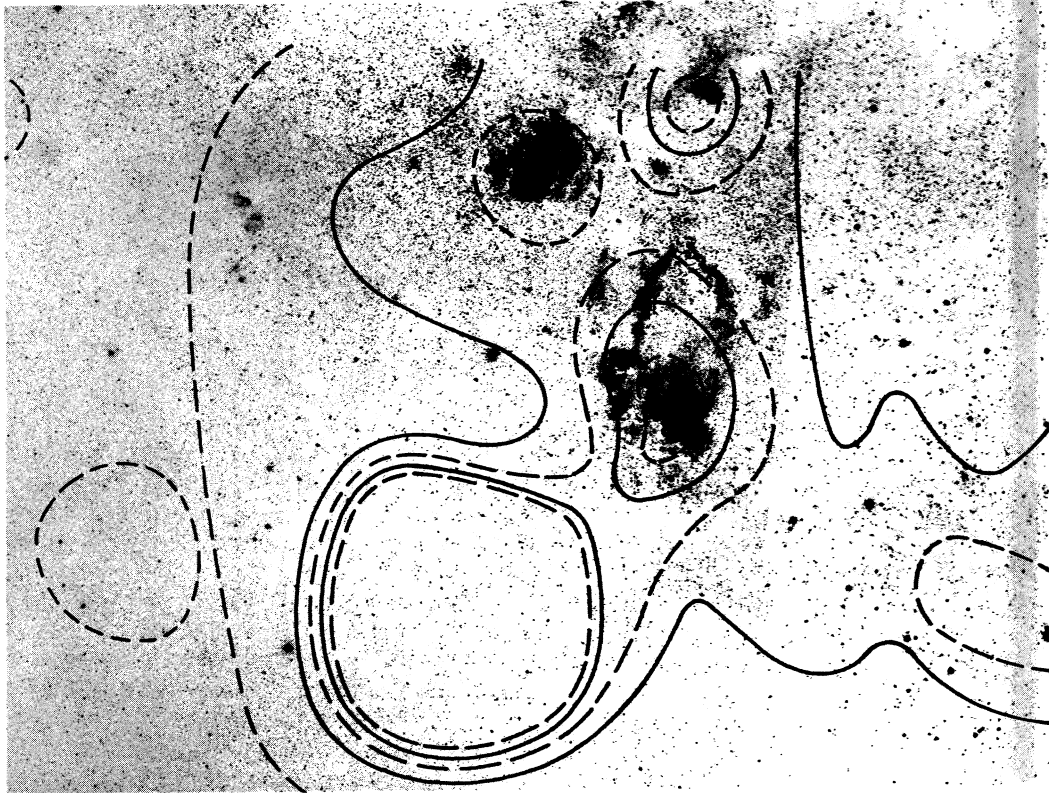
Fig. 12. —— The region of NGC 7000. The radio brightness contours of Figure 5 are shown here superimposed on the corresponding optical field reproduced from "E" emulsion prints of the National Geographic **Society Sky** Atlas.

60

Fig. 13. —— The region of IC 1396. The radio brightness contours of Figure 6 are shown here superimposed on the corresponding optical field reproduced from "E" emulsion prints of the National Geographic Society Sky Atlas.

Fig. 14. —— The region of Cas A. The radio brightness contours of Figure 7 are shown here superimposed on the corresponding optical field reproduced from "E" emulsion prints of the National Geographic Society Sky Atlas.